IEEE Access
Multidisciplinary | Rapid Review | Open Access Journal

Received 18 December 2023, accepted 23 January 2024, date of publication 26 January 2024, date of current version 2 February 2024.

Digital Object Identifier 10.1109/ACCESS.2024.3359112

RESEARCH ARTICLE

Improvement of the Pointing Accuracy of Shipborne Optical Measuring Equipment Based on a Subdivision Iteration Algorithm

XIN HUANG[1,2], JING WANG[1], DONG WANG[3], JIAHAO PENG[1], AND BAO ZHAO[1,2]
[1]Changchun Institute of Optics, Fine Mechanics and Physics, Chinese Academy of Sciences, Changchun 130033, China
[2]Department of Mechanical Manufacturing and Automation, University of Chinese Academy of Sciences, Beijing 100049, China
[3]China North Vehicle Research Institute, Beijing 100072, China

Corresponding author: Jing Wang (wangjing@ciomp.ac.cn)

This work was supported in part by the National Natural Science Foundation of China under Grant 51675506, and in part by the Jilin Province Excellent Young Talent Fund under Grant 20190103015JH.

ABSTRACT When performing measurement and control tasks at sea, the optical measuring equipment on an aerospace survey ship must demonstrate a high pointing accuracy. Ideally, a fixed sequence of ''yaw–pitch–roll'' is used to perform the coordinate transformation from the Earth reference system to the deck coordinate system, introducing a coordinate transformation error. This study proposes a parametric model based on the subdivision iterative algorithm to correct the errors of the coordinate–transformation sequence of the ship's attitude and systematic errors caused by the coupling of several error sources to improve the pointing accuracy of the space–measurement equipment on a ship. Star-tracking experiments verify the validity of the model. Compared with the existing models, the proposed pointing–error model reduces the corrected residual from 42″to 18.4″and the open-loop pointing error from 11.5″to 8.1″. The results show that the application of the proposed model helped improve the pointing accuracy of the optical measuring equipment after correction. These findings could prove significant for similar studies on goniometric precision and data processing accuracy.

INDEX TERMS Coordinate–transformation error, optical measuring equipment, pointing–error analysis, star–tracking experiments.

I. INTRODUCTION

The aerospace survey fleet possesses comprehensive solid measurement and control capabilities, is flexible and mobile, and can provide measurement and control support for various space-launch test missions. Unlike measurements performed by land-based stations and other moving platforms, space-survey ships face a complex marine environment when performing maritime measurements and control tasks. Therefore, achieving high pointing accuracy is difficult for shipborne optical measurement systems under random and violent oscillation conditions at sea. The equipment itself displays unavoidable systematic errors. In addition, excessively harsh requirements on the hardware, through the use of high-precision equipment and mechanical manufacturing processes, to reduce the pointing error, are not only technically challenging to realize but also uneconomical. The pointing error of the equipment has a certain regularity and must thus be modeled and analyzed [1], [2].

Ships will periodically yaw, pitch and roll under the action of wind, waves and ocean currents. Therefore, the research on the pointing error of shipborne optical measuring equipment belongs to the research category of moving

The associate editor coordinating the review of this manuscript and approving it for publication was Hassen Ouakad.

platform pointing, but it is also based on fixed platform. The geometric error and sensor error are the primary sources of error for fixed platforms [3], [4]. The existing fixed platform pointing research usually adopts the method of building parameter model to correct the pointing error. Yan et al. [5] used a parametric model based on Allan's variance to eliminate geometric errors, significantly improving the Alt-az telescope's pointing accuracy. Zhang et al. [6] analyzed the geometric error sensitivity of the pointing accuracy of an acquisition pointing and tracking (APT) system using a multibody kinematics-based method. They conducted correction experiments based on the pointing-error distribution law of the simulation results and achieved improved pointing accuracy. He et al. [7] proposed a new optimized parameter model to improve the pointing accuracy of Mobile Platform Electro-Optical Telescope (MPEOT). They developed a linear pointing-correction model based on the target localization process. Therefore, they could eliminate multiple covariances and obtain the optimized parameter model using the stepwise regression method. The experimental results show that the model-corrected MPEOT is better than the coordinate model, with a pointing error of less than 50 arcs in approximately 23 h. Huang et al. [8] established a simulation model of the pointing error based on the Monte Carlo method as well as the distribution of the pointing error before and after the correction of the assembling error. The results of the correction experiments showed an average of 64% improvement in the pointing accuracy. Hong et al. [9] developed a parametric model to eliminate the pointing accuracy of the geometric and sensor error of a two-degree-of-freedom miniature inertial stabilized platform. Zhou et al. [10] analyzed the mechanical error of an aerial camera, established a pointing-error model based on ray tracing, and used genetic algorithms for parameter identification. They experimentally demonstrated significant improvements in the pointing accuracy of the line-of-sight (LOS) after using the pointing-error model.

Unlike fixed platforms, the inertial navigation system of the moving platform is equipped with attitude sensor, which can obtain the attitude and position information of the measuring ship. In addition, subject to changes in the ship's attitude, the LOS of the shipborne optical measuring equipment is subject to swaying [11]. Therefore, the target's position must be aligned in the Northeast celestial coordinate system (Fig.1) with the deck coordinate system. In Fig.1, the x-, y-, and z-axes point toward due east, due north, and the sky, respectively, and origin O represents the intersection of the azimuth axis of the photometric equipment and the pitch axis. Furthermore, the polar coordinates of the observation target M are denoted as (A, E), where$A$ denotes the azimuth angle, which is positive for a clockwise view, and E denotes the pitch angle. Moreover, L is the distance from the photometric equipment to the observation target, M.

In the process of coordinate alignment, a fixed sequence, i.e., ''yawing, pitching and rolling'' is commonly used for

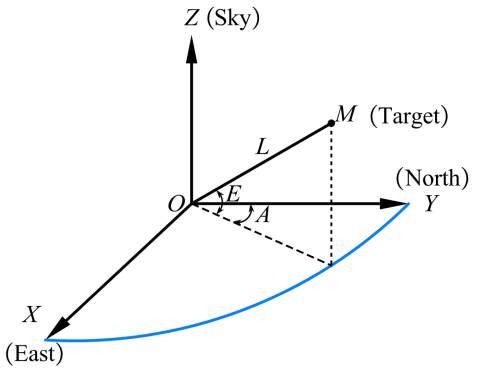

FIGURE 1. Northeast celestial coordinate system.

coordinate conversion at present [12], [13], [14]. However, the sequence for measuring the three directions of the ship's rocking motion is yet to be determined. In addition, the sequence for transmitting the rocking data measured by the gyro sensors in the three directions to the central control computer is unknown. Hence, the accuracy of the fixed line of the coordinate conversion must be further verified [15], [16]. Wang [17] exchanged the results of the transformation sequence of the transverse and longitudinal rocking and pointed out that the ship's rocking is a combination of both. Zhou et al. [18] simulated and highlighted the effect of predicting and tracking the target according to the ''yaw, pitch, and roll'' order in class 5 or above sea state, achieving generalized results. Therefore, it is considered that the position coordinates obtained by using the fixed coordinate conversion sequence cannot accurately describe the position of the target in the deck coordinate system. Meanwhile, the inertial guidance system for measuring the ship's attitude and position will introduce installation errors during installation, and the attitude sensor itself will also have sensor errors. These error sources and the error incurred by the coordinate conversion sequence were coupled, thus reducing the pointing accuracy. He et al. [19] calibrated the installation and geometric errors separately in satellite-to-sea laser-communication-tracking-and-pointing experiments but could not simultaneously calculate the error parameters. Peng et al. [20] proposed a method that can avoid many errors for gimbal-type optical communication terminal, which is the most effective means for predicting target tracking. They proposed a pointing model that can avoid the coupling of many errors and verified its validity through experiments; however, they did not consider the errors caused by the order of coordinate transformation.

In this paper, we present a new mathematical model based on pointing errors that corrects the errors caused by the order of the coordinate transformation and avoids the coupling with geometric errors, sensor errors and other error sources. Star-tracking experiments were conducted to verify the model, showing a significant improvement in the pointing accuracy.

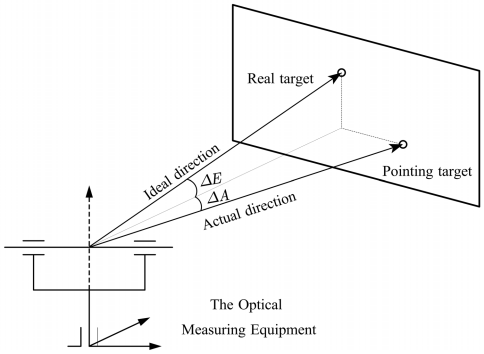

FIGURE 2. Schematic of the pointing error.

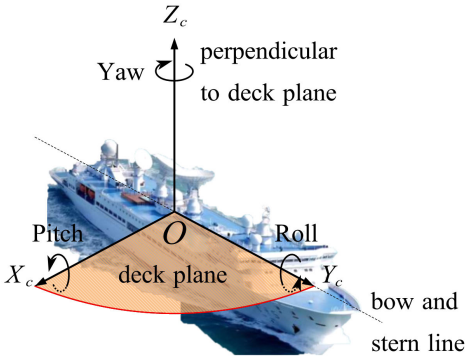

FIGURE 3. Coordinate system of the deck of a ship.

II. ERROR-SOURCE ANALYSIS AND MODELING

A. ERROR-SOURCE ANALYSIS

As the optical measurement equipment is installed on the measurement ship, it cannot accurately provide the position and attitude information of the equipment base; this information must therefore be gained from the inertial guidance system. However, the information provided by the inertial guidance system will have a specific measurement error, inevitably resulting in the introduction of a coordinate conversion error. In addition, the equipment itself demonstrates a systematic error. The shipboard optical measurement equipment controls the rotation of the azimuth and pitch axes to control the optical axis pointing to the target for tracking; these axes constitute the measurement coordinate system, the origin of which is the intersection of the three axes. Goniometric errors occur when the azimuth axis is not perpendicular to the deck coordinate system reference plane, the pitch axis is not perpendicular to the azimuth axis, or the optical axis is not perpendicular to the pitch axis. The goniometric error caused by the tilt of the azimuth, pitch and optical axes and the non-perpendicularity between them constitutes the axis system error. The axis and encoder errors together constitute the system error of the device.

As shown in Fig. 2, because of the existence of coordinate translation errors and systematic errors, the components of the difference between the actual pointing direction of the device LOS and the ideal pointing direction in the azimuth and pitch axes are defined as the pointing errors of the device in the azimuth and pitch axes, respectively, which are determined as follows:

$$\begin{cases} \Delta A = A - \hat{A} = f(A, E) + \varepsilon \\ \Delta E = E - \hat{E} = g(A, E) + \tau \end{cases} \tag{1}$$

where ΔA and ΔE are pointing errors on the azimuth and pitch axes, respectively; $\hat{A}$ and $\hat{E}$ are the encoder measurements on the azimuth and elevation axes, respectively; A and E are the actual pointing values of the device; $f(A, E)$ and $g(A, E)$ denote the pointing-error functions, with A and E as independent variables; and ε and τ are residuals.

B. ERROR-SOURCE MODELING

1) COORDINATE CONVERSION ERROR

Kinematic modeling showed that the ship position and systematic equipment errors are related to the actual pointing LOS, and each error source was calibrated during star-tracking. Fig.3 defines the deck coordinate system, $O - X_c Y_c Z_c$, with the OY_c axis representing the bow and stern lines, pointing toward the ship's bow. Furthermore, the OZ_c axis is perpendicular to the deck plane in the upward direction, and the right-hand rule defines the OX_c axis and points to the starboard in the deck plane.

The Denavit–Hartenberg (D–H) method is usually used to describe the rotation and translation between objects. When using the equipment, as the observation target is usually far away and the effect of the small-distance translation on the pointing error is negligible, a third-order matrix containing the transformation angle can be used to favorably define the attitude of the equipment and the angular transformation related to the LOS. In this paper, the coordinate system rotation matrices for the yaw, pitch, and roll are represented as follows:

$$\begin{aligned} R_h &= \begin{bmatrix} \cos H & -\sin H & 0 \\ \sin H & \cos H & 0 \\ 0 & 0 & 1 \end{bmatrix} \\ R_p &= \begin{bmatrix} 1 & 0 & 0 \\ 0 & \cos P & \sin P \\ 0 & -\sin P & \cos P \end{bmatrix} \\ R_r &= \begin{bmatrix} \cos R & 0 & -\sin R \\ 0 & 1 & 0 \\ \sin R & 0 & \cos R \end{bmatrix} \end{aligned} \tag{2}$$

The attitude angle R, P, and H of the survey vessel is illustrated in Fig.4. Moreover, the ship's rocking is described by three quantities: (1) pitch angle P, which represents the longitudinal rocking of the ship, with the bow high and positive; (2) roll angle R, which represents the ship's rocking from side to side, with the port side rising and cheerful; and (3) yaw angle H, which represents the angle of the bow and stern lines due north; the yaw angle is positive when viewed downward from the direction of the mast and is positive when viewed clockwise.

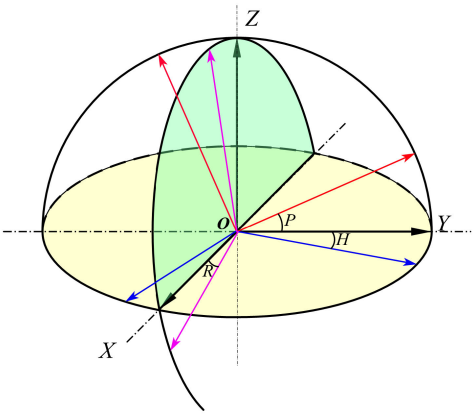

FIGURE 4. Schematic of the attitude angle.

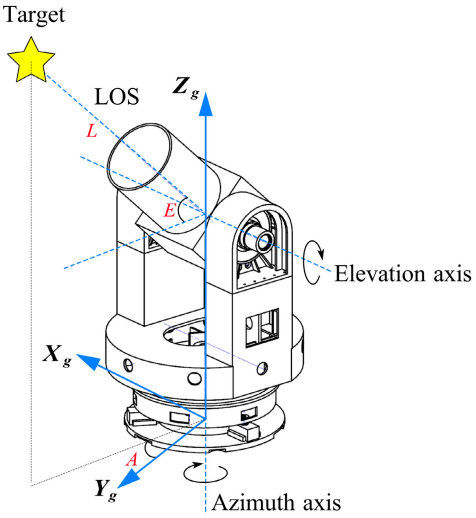

FIGURE 5. Coordinate system of the sensor mounted on the device.

The coordinate system of the attitude sensor mounted on the device is presented in Fig. 5. From the direction of the rotation axis, the azimuth angle is positive in the clockwise direction. In addition, the rotation range of the azimuth axis is 0°-360°, the pitch angle is positive counterclockwise, and the rotation range of the pitch axis is 0°-90°. When the device does not receive a perturbation, the attitude sensor coordinates the system's x-, y-, and z-axes to coincide with the device's elevation axis, LOS, and azimuth axis, respectively.

The optical measuring equipment has the capability of automated calibration of stars. In this study, stars with precise positions were used as observation targets and the selected stars should be uniformly distributed in the space with an azimuth of 0°–360° and an elevation angle of 20°–60°. The theoretical guide values of the observed stars (A_n, E_n) were converted into the pointing vectors of the LOS of the equipment $(x_n, y_n, z_n)^T$:

$$\begin{cases} x_n = \cos E_n \sin A_n \\ y_n = \cos E_n \cos A_n \\ z_n = \sin E_n \end{cases} \tag{3}$$

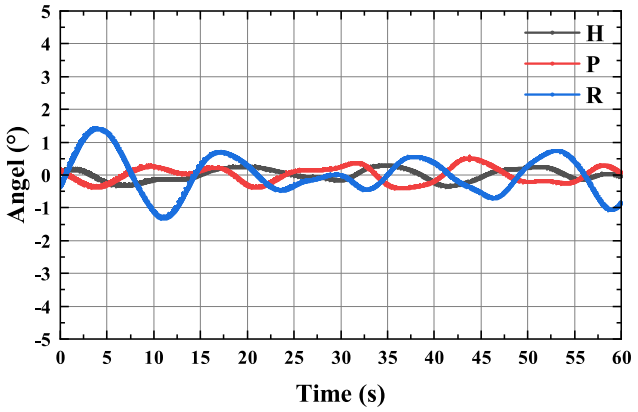

FIGURE 6. Angle change of the optical measuring-equipment base.

According to the ship's attitude and position information measured by the inertial guidance system, the position of the observation target was transformed from the Northeast celestial coordinate system to the deck coordinate system. The most commonly used method involves the transformation of the coordinate system in the order of "yaw–pitch–roll," i.e., the coordinate transformation is performed as

$$(x_g, y_g, z_g)^T = R_r R_p R_h (x_n, y_n, z_n)^T \tag{4}$$

When the measurement ship operates at sea, perturbations from all directions are simultaneously observed, and if the target position coordinates are solved according to the artificially specified sequential conversion, coordinate conversion errors are introduced. In this study, a single star was targeted in the star-tracking experimental ocean, and when the LOS of the photometric equipment was pointed at the target star, the azimuth angle of the target position was measured as 45.0269° and the pitch angle was measured as 35.2644°. The inertial guidance information of the survey ship was recorded, resulting in the angular change of the photometric equipment base, as shown in Fig.6. Furthermore, the apparent axis angles obtained by solving using six coordinate conversion sequences are shown in Fig.7

The simulation results showed that the view axis angles obtained from different conversion sequences differed because the pointing angle of the LOS was rotated by the coordinate axis of the previous converted coordinate system during the conversion process. In addition, the actual inertial guidance information was based on a fixed geocentric solid coordinate system. Furthermore, the rotation according to different reference axes could introduce a coordinate conversion error, resulting in different pointing angles of the LOS. However, the measurement vessel only displayed one final attitude after swinging. Hence, we adopted a subdivision-based iterative method to replace the original fixed transformation order for coordinate transformation to obtain the closest genuine attitude of the measurement vessel. Specifically, the initial transformation angle was subdivided into n equal parts, and the slight angle could transform the LOS to simulate the actual situation of the ship rocking

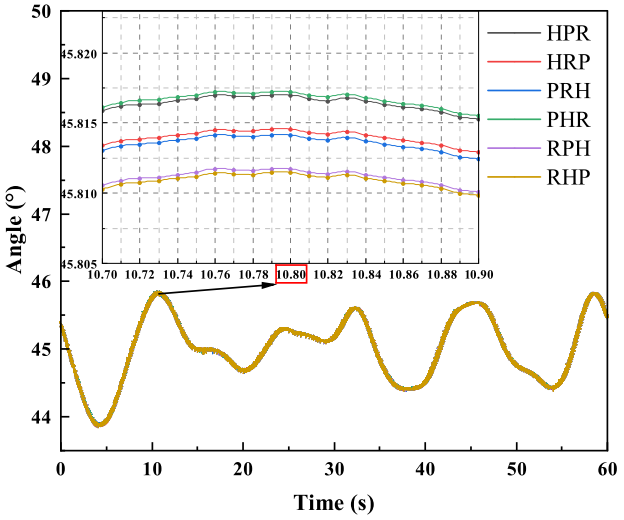

(a) Simulation results of the azimuth angle.

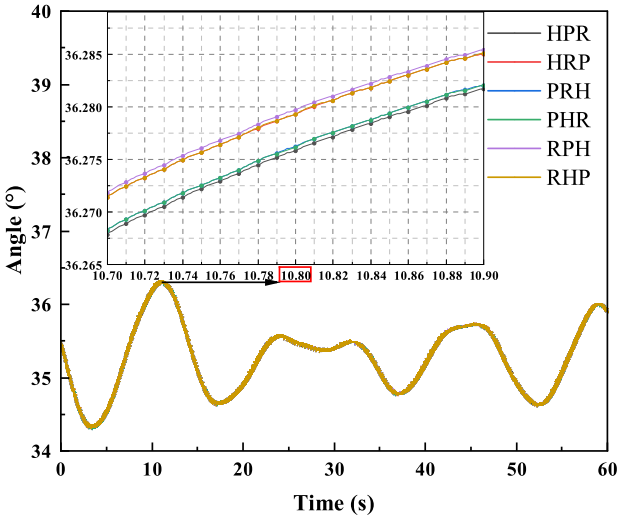

(b) Simulation results of elevation angle.

FIGURE 7. Effect of different coordinate-transformation sequences on the azimuth and elevation angles.

disturbance in all directions simultaneously. This expression is represented as

$$\left(x_g, y_g, z_g\right)^T = \left[R_r\left(\frac{R}{n}\right) R_p\left(\frac{P}{n}\right) R_h\left(\frac{H}{n}\right)\right]^n \left(x_n, y_n, z_n\right)^T \tag{5}$$

When n=1, it represents a commonly used coordinate conversion order. Then, n is considered as 10,100,1000 to simulate the azimuth and pitch angles, as shown in Fig.8. The azimuth and elevation angles obtained from the six coordinate conversion sequences gradually approach the actual values with increasing n. The computational scale of the subdivision iterative algorithm increases with n. In addition, time required to solve individual coordinates and the conversion order error is listed in Table 1.As shown, when n=1000, the error introduced by the different conversion orders of the azimuth and pitch angles was at its maximum of 0.02″,demonstrating

TABLE 1. Effect of change in n on the time and errors of the coordinate-transformation sequence.

n	1	10	100	1000
Time(ms)	1.8	2.0	2.3	2.7
errors of the coordinate transformation sequence(″)	20.7	2.1	0.2	0.02

TABLE 2. Summary of error sources.

Error sources	Symbol	Matrix	Rotation axis
Optical axis tilts toward x-axis	γ_z	R_{Mz}	Z
Optical axis tilts toward z-axis	γ_x	R_{Mx}	X
Flexure	δ_T	R_F	X
Elevation encoder errors	$E, E_{\beta 1}, E_{\beta 2}$	R_E	Z
Elevation bearing tilts toward z-axis	$\xi_{B1}\cos E$	R_{B1}	Y
Nonorthogonality of azimuth and elevation axis	η	R_N	Y
Azimuth encoder errors	$A, A_{\beta 1}, A_{\beta 2}$	R_A	X
Elevation bearing tilts toward y-axis	$\xi_{B2}\cos E$	R_{B2}	Z
Azimuth bearing tilts toward y-axis	$\xi_{B3}\cos A$	R_{B3}	X
Azimuth bearing tilts toward x-axis	$\xi_{B4}\cos A$	R_{B4}	Y

a higher accuracy by the algorithm than solving using a fixed sequence of coordinate conversion. As the communication frequency of the shipboard optical measurement equipment was 100 Hz and the main control time between each frame was 10 ms, the algorithm could meet the usage requirements even when n=1000.

Next, the attitude sensor was mounted on the device and the equipment was mounted on the deck. When converting the LOS pointing vectors to the measuring coordinate system of the device, the mounting errors of the sensor must be considered, which can be eliminated by rotating the matrix (6).

$$\begin{aligned} R_\phi &\approx \begin{bmatrix} 1 & 0 & -\alpha_1 \\ 0 & 1 & 0 \\ \alpha_1 & 0 & 1 \end{bmatrix} \begin{bmatrix} 1 & 0 & 0 \\ 0 & 1 & \alpha_2 \\ 0 & -\alpha_2 & 1 \end{bmatrix} \begin{bmatrix} 1 & -\alpha_3 & 0 \\ \alpha_3 & 1 & 0 \\ 0 & 0 & 1 \end{bmatrix} \\ &\approx \begin{bmatrix} 1 & -\alpha_3 & -\alpha_1 \\ \alpha_3 & 1 & \alpha_2 \\ \alpha_1 & -\alpha_2 & 1 \end{bmatrix} \end{aligned} \tag{6}$$

where α_1, α_2, and α_3 are the error angles between the measurement axis of the sensor and pointing axis of the photometric device.

2) SYSTEMATIC-ERRORS MODEL

The systematic error comprises the axis system and encoder errors, i.e., in the case of an error term, the LOS is rotated by one angle. Therefore, the error terms and rotation matrix are summarized in the order of the occurrence of the coordinate transformation of the LOS pointing accuracy (LOS—elevation axis—azimuth axis—base), as shown in Table 2.

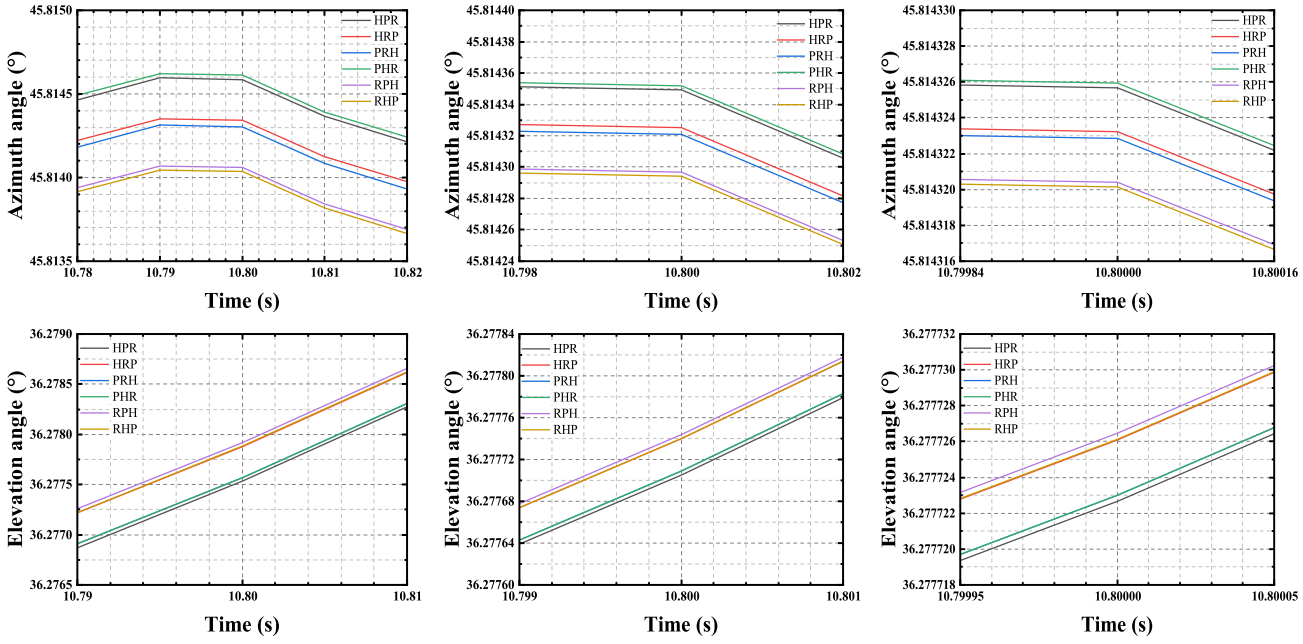

(a) n=10 (b) n=100 (c) n=1000

FIGURE 8. Effect of change of *n* on the azimuth and elevation angles.

The encoder errors include zero position, scale, and eccentricity errors. As shown in Table 2, $A_{\beta 1}$ and $E_{\beta 1}$ represent zero errors of the azimuth and elevation angles, respectively. The sum of each encoder-scale error and eccentricity error is defined by $A_{\beta 2}$ and $E_{\beta 2}$, respectively, where the scale error is related to the current encoder value and represented as $m_1 A/2\pi$ and $n_1 E/2\pi$. Moreover, the eccentricity of the code disk and slit introduces the eccentricity error of the encoder, and the shaking during the rotation of the equipment exacerbate the degree of abnormality, thus affecting the accuracy of the encoder. In general, $m_2 \sin A$ and $m_3 \cos A$ are used to express the eccentricity error of an azimuth encoder in the x- and y- axis directions of the shaft, and $m_2 \sin A$ and $m_3 \cos A$ are commonly used for describing the eccentricity error of a pitch encoder in the z- and y-axis directions. Therefore, we have

$$\begin{cases} A_{\beta 2} = m_1 A/2\pi + m_2 \sin A + m_3 \cos A \\ E_{\beta 2} = n_1 E/2\pi + n_2 \sin E + n_3 \cos E \end{cases} \tag{7}$$

Therefore, the LOS is rotated about the azimuth axis by an angle of $A + A_{\beta 1} + A_{\beta 2}$ and around the pitch axis by an angle of $E + E_{\beta 1} + E_{\beta 2}$. Thus, we have

$$\begin{aligned} R_A &= \begin{bmatrix} \cos\left(A + A_{\beta 1} + A_{\beta 2}\right) & \sin\left(A + A_{\beta 1} + A_{\beta 2}\right) & 0 \\ -\sin\left(A + A_{\beta 1} + A_{\beta 2}\right) & \sin\left(A + A_{\beta 1} + A_{\beta 2}\right) & 0 \\ 0 & 0 & 1 \end{bmatrix} \\ &\approx R_{A\beta 1} R_{A\beta 2} \end{aligned} \tag{8}$$

where

$$R_{A\beta 1} = \begin{bmatrix} 1 & A_{\beta 1} & 0 \\ -A_{\beta 1} & 1 & 0 \\ 0 & 0 & 1 \end{bmatrix}$$

$$R_{A\beta 2} = \begin{bmatrix} \cos A - A_{\beta 2} \sin A & \sin A + A_{\beta 2} \cos A & 0 \\ -\sin A - A_{\beta 2} \cos A & \cos A - A_{\beta 2} \sin A & 0 \\ 0 & 0 & 1 \end{bmatrix}$$

III. DERIVATION OF THE POINTING MODEL

The modeling of the pointing error can help determine each error parameters by backtracking the coordinates of the observations in the order in which the errors appear and making them point to the same direction as the LOS of the equipment. The position of the observation target is converted from the Northeast celestial coordinate system to the sensor coordinate system of the equipment according to (5). The position must then be converted to the base coordinate system of the equipment by considering the mounting error, as shown in (6). In the case of no systematic error influence on the equipment, the LOS optic axis ideally points to $(0, 1, 0)^T$. Then, the coordinate conversion of vector rotation is performed in the order of the occurrence of the error sources summarized in 2 and finally converted to the same base coordinate system as that of the observation target. Here, the LOS of the equipment was considered to point to the ideal direction after the influence of the various error terms. The process is represented by (9), wherein the rotation matrices are all simplified using the small-angle approximation:

$$\begin{aligned} R_\phi \left(x_g, y_g, z_g\right)^T &= R_{B4} R_{B3} R_{B2} R_A R_N R_{B1} \\ &\times R_E R_F R_{Mx} R_{Mz} (0, 1, 0)^T \end{aligned} \tag{9}$$

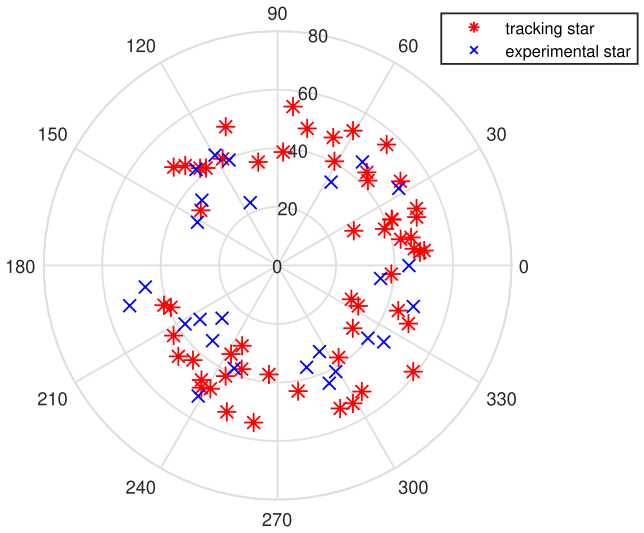

FIGURE 9. Star-map distribution used in the experiment.

The ideal pointing direction of the device is the direction in which the encoder value is guided, and the pointing direction is denoted as

$$\begin{cases} x = \cos E \sin A \\ y = \cos E \cos A \\ z = \sin E \end{cases} \tag{10}$$

The pointing vector error is obtained by substituting (9) and (10) into (11):

$$\begin{bmatrix} \Delta x \\ \Delta y \\ \Delta z \end{bmatrix} = \begin{bmatrix} x_g \\ y_g \\ z_g \end{bmatrix} - \begin{bmatrix} x \\ y \\ z \end{bmatrix} = B \cdot \vec{c} \tag{11}$$

where, as shown in the equation at the bottom of the next page,

$\vec{c}$ is a vector of error parameters:

$$\vec{c} = [\alpha_1, \alpha_2, \alpha_3 + A_{\beta 1}, E_{\beta 1} + \gamma_x, \gamma_z, \delta_T, \eta, \xi_{B1}, \xi_{B2}, \xi_{B3}, \xi_{B4}, m_1, m_2, m_3, n_1, n_2, n_3]^T$$

The parameters in the parameter vector $\vec{c}$ are calibrated by shooting stars, using the least squares method as in (12):

$$\vec{c} = \left(B^T B\right)^{-1} B^T \left(x_z, y_z, z_z\right)^T \tag{12}$$

Bringing (8) into (9) yields the following equation:

$$R_{A\beta 1}^T R_\phi \left(x_g, y_g, z_g\right)^T = R_{B4} R_{B3} R_{B2} R_{A\beta 2} R_N R_{B1} R_E R_F R_{Mx} R_{Mz} (0, 1, 0)^T \tag{13}$$

The guide value can be calculated from (14)-(18):

$$\left(x_c, y_c, z_c\right)^T = R_{A\beta 1}^T R_\phi \left(x_g, y_g, z_g\right)^T \tag{14}$$

$$\left(x_p, y_p, z_p\right)^T = R_{B4} R_{B3} R_{B2} R_{A\beta 2} R_N R_{B1} \times R_E R_F R_{Mx} R_{Mz} (0, 1, 0)^T \tag{15}$$

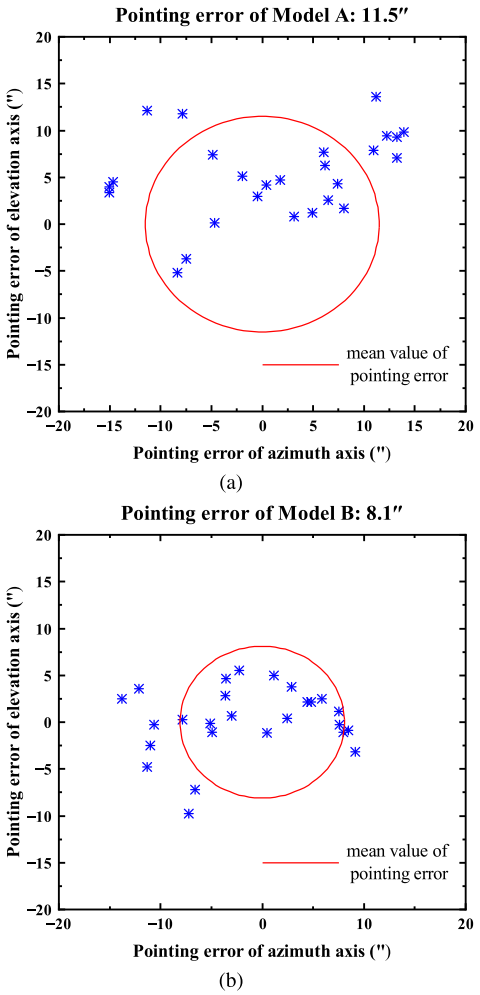

FIGURE 10. Open-loop pointing errors in (a) Model A and (b) Model B.

$$A_c = \arctan\left(\frac{x_c}{y_c}\right), E_c = \arcsin z_c \tag{16}$$

$$A + \Delta A_c = \arctan\left(\frac{x_p}{y_p}\right), E + \Delta E_c = \arcsin z_p \tag{17}$$

$$A + \Delta A_c = A_c, E + \Delta E_c = E_c \tag{18}$$

Therefore, the pointing error is obtained as shown in equation (20):

$$\begin{aligned} \Delta A_c = {} & \gamma_z \sec E_c - \eta \tan E_c - \xi_{B1} \sin E_c + \xi_{B2} \cos E_c \\ & + \xi_{B3} \sin A_c \cos A_c \tan E_c + \xi_{B4} \cos^2 A_c \tan E_c \\ & + m_1 A_c / 2\pi + m_2 \sin A_c + m_3 \cos A_c \\ \Delta E_c = {} & E_{\beta 1} + \gamma_x + \delta_T \cot E_c - \xi_{B4} \sin A_c \cos A_c \\ & + n_1 E_c / 2\pi + n_2 \sin E_c + n_3 \cos E_c + \xi_{B3} \cos^2 A_c \end{aligned} \tag{19}$$

IV. EXPERIENCE AND RESULTS

The experimental object was the ocean-going space optical measuring equipment with a diameter of 400 mm developed by Changchun Institute of Optics, Fine Mechanics and

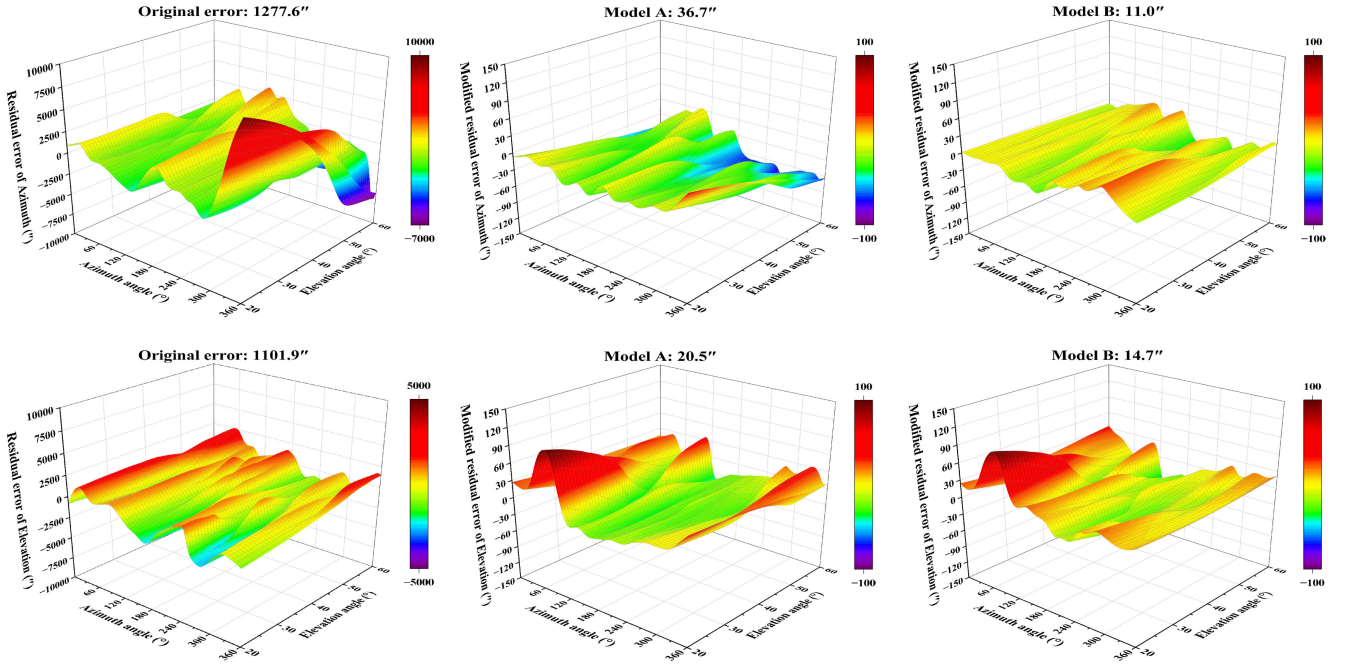

(a) Total original error: 1687.1″. (b) Total residuals error : 42″. (c) Total residuals error : 18.4″.

FIGURE 11. (a) Uncorrected original error, and residual errors corrected for (b) model A and (c) model B.

Physics, Chinese Academy of Sciences. The goal was to verify the feasibility of the proposed mathematical model based on the subdivision iterative method (called model B) and compare it with the model presented in literature (called model A) [20]. The two mathematical models to be compared were integrated into the monitoring subsystem of optical measuring equipment. The stars were tracked using optical measuring equipment to obtain the actual pointing of the LOS. Then, a different batch of other stars was tracked to validate the comparison of the open-loop pointing accuracy of the two models. Fig.9 shows that the measured stars are uniformly distributed in the four quadrants of space.

The measurement ship was driven to the sea experiment area (30°41.816′N, 122°30.633′E) for star tracking. The experiment was divided into two phases. (1) In the first phase, the information of 56 stars was tracked and measured to calibrate the pointing capability of the optical measuring equipment. When the principal analysis entered the field of view of the charge-coupled device (CCD) TV, the optical measuring equipment automatically recorded the star's

$$B = \begin{bmatrix} \sin E & 0 & -\cos E \sin A \\ 0 & -\sin E & \cos A \cos E \\ \cos A \cos E & -\sin A \cos E & 0 \\ -\sin A \sin E & -\cos A \sin E & \cos E \\ \cos A & -\sin A & 0 \\ -\cos E \sin A & -\cos A \cos E & \cos E \cot E \\ -\cos A \sin E & \sin A \sin E & 0 \\ -\cos A \cos E \sin E & \cos E \sin A \sin E & 0 \\ \cos A \cos^2 E & -\cos^2 E \sin A & 0 \\ 0 & -\cos A \sin E & \cos^2 A \cos E \\ \cos A \sin E & 0 & -\cos A \cos E \sin A \\ A \cos A \cos E/2\pi & -A \cos E \sin A/2\pi & 0 \\ \cos A \cos E \sin A & -\cos E \sin^2 A & 0 \\ \cos^2 A \cos E & -\cos A \cos E \sin A & 0 \\ -E \sin A \sin E/2\pi & -E \cos A \sin E/2\pi & E \cos E/2\pi \\ -\sin A \sin^2 E & -\cos A \sin^2 E & \cos E \sin E \\ -\cos E \sin A \sin E & -\cos A \cos E \sin E & \cos^2 E \end{bmatrix}^T$$

positional angle in the Northeast celestial spherical coordinate system (A_n, E_n) and the equipment's attitude and the encoder's value (A, E). Each star measured 100 points, and selected 11 consecutive points of data for center smoothing. The acquired data were used to calibrate the error parameters of the photometric device using model A and model B respectively and the residuals corrected by the two models were obtained as shown in Fig.11. (2) In the next phase, we performed open-loop tracking of another 26 stars using shipboard photometric equipment and obtained open-loop pointing accuracies for models A and B. The obtained results are shown in Fig.10, where the original error before the correction is 1687.1″, and the residuals are obtained as 42″ and 18.4″ after the correction using models A and B, respectively.

The total pointing error is calculated as follows: (20):

$$\delta_{total} = \sqrt{\delta_{azimuth}^2 + \delta_{elevation}^2} \tag{20}$$

According to the experimental results, the corrected residual of model B was 18.4″ and that of model A was 42″. In addition, the open-loop pointing errors of models B and A were obtained as 8.1″ and 11.5″, respectively. Based on the proposed subdivision iteration algorithm, model B improved the pointing accuracy of the optical measuring equipment on the shipboard platform after correcting the coordinate conversion sequence error.

V. CONCLUSION

The coordinate conversion error is a human-introduced error, which can also be coupled with systematic errors, thus reducing the pointing accuracy of the optical measurement equipment of a platform in motion. This study numerically simulated different coordinate conversion sequences of the ship's posture to compare and analyze their influence on the accuracy of the measured azimuth and pitch angles. The original fixed "yaw–pitch–roll" conversion sequence was replaced using a subdivided and iterative method to simulate the actual occurrence of the ship's rocking motion. A mathematical model of the pointing error was proposed to improve the pointing accuracy of the optical measuring equipment by subdividing and iterating instead of the original fixed "yaw–pitch–roll" conversion sequence to simulate a ship's actual rocking motion. Furthermore, star-tracking experiments were conducted to verify the validity of the model. The uncorrected and original error was 1687.1″, and the residual error after performing corrections using the existing model was 42″. By contrast, the proposed pointing-error model reduced the corrected residual error from 42″ to 18.4″, and the open-loop pointing error was reduced from 11.5″ to 8.1″. Thus, the proposed model could improve the pointing accuracy of the optical measuring equipment on a shipboard platform. The model has generalization ability and adaptability, and can be applied to similar two-degree-of-freedom devices.

REFERENCES

[1] Y. Wang, Z. Lou, Y.-X. Zuo, H.-R. Kang, and M.-Z. Zhang, "Study on the pointing model of a slant-axis terahertz antenna," *Res. Astron. Astrophys.*, vol. 20, no. 4, p. 57, Apr. 2020.
[2] K.-P. Sung, H.-C. Lim, J.-U. Park, M.-S. Choi, S.-Y. Yu, E.-S. Park, and J.-C. Ryou, "Pointing accuracy analysis of space object laser tracking system at geochang observatory," *J. Korean Soc. Aeronaut. Space Sci.*, vol. 49, no. 11, pp. 953–960, Nov. 2021.
[3] C. Xu, W. Han, D. Wang, D. Huang, and P. Yuan, "Modeling and correction for the optical axis pointing error of an airborne electro-optical platform," *Appl. Opt.*, vol. 58, no. 23, p. 6455, 2019.
[4] Q. Tang, Q. Yang, X. Wang, and A. B. Forbes, "Pointing error compensation of electro-optical detection systems using Gaussian process regression," *Int. J. Metrol. Quality Eng.*, vol. 12, p. 22, Jan. 2021.
[5] L. Yan, Y. Huang, and Y. Zhang, "Using Allan variance based semi-parameter model to calibrate pointing errors of alt-az telescopes," *Appl. Sci.*, vol. 8, no. 4, p. 614, Apr. 2018.
[6] F. Zhang, P. Ruan, J. Han, and Y. Li, "Analysis and correction of geometrical error-induced pointing errors of a space laser communication APT system," *Int. J. Optomechatronics*, vol. 15, no. 1, pp. 19–31, Jan. 2021.
[7] Y. He, Y. Zhang, X. Feng, S. Deng, and Z. Wang, "Pointing error correction for a moving-platform electro-optical telescope using an optimized parameter model," *Sensors*, vol. 23, no. 8, p. 4121, Apr. 2023.
[8] B. Huang, Z. H. Li, X. Z. Tian, L. Yang, P. J. Zhang, and B. Chen, "Modeling and correction of pointing error of space-borne optical imager," *Optik*, vol. 247, Dec. 2021, Art. no. 167998.
[9] H. Hong, X. Zhou, Z. Zhang, and D. Fan, "Modeling and calibration of pointing errors using a semi-parametric regression method with applications in inertially stabilized platforms," *Proc. Inst. Mech. Eng., B, J. Eng. Manuf.*, vol. 227, no. 10, pp. 1492–1503, Oct. 2013.
[10] X. Zhou, H. Liu, Q. Liu, and J. Lin, "Modeling and optimization of the integrated TDICCD aerial camera pointing error," *Appl. Opt.*, vol. 59, no. 27, p. 8196, 2020.
[11] D. P. O'Leary and D. A. Schug, "Achieving a common view point: Yaw, pitch, and roll," *Comput. Sci. Eng.*, vol. 6, no. 5, pp. 60–62, Sep. 2004.
[12] X. Zhenkai and C. Tingfeng, "High-precision tracking and pointing control technique," *High Power Laser Part. Beams*, vol. 24, no. 6, pp. 1339–1343, 2012.
[13] F. Yiyan and Z. Bin, "Coordinate measurement based on attitude angle sensor and rotating rangefinder," *Infr. Laser Eng.*, vol. 45, no. 1, 2016, Art. no. 117001.
[14] Z. Xuehan, W. Zhenzhong, and Z. Guangjun, "Expeditions calibration algorithm of visual tracking and measurement system with field coordinate system for moving target," *Infr. Laser Eng.*, vol. 44, no. 7, pp. 2175–2181, 2015.
[15] L. Erwei, "Research on stabilization algorithm of los for ship borne laser weapon based on the strap down measurements," *Proc. SPIE*, vol. 11334, pp. 307–312, Feb. 2019.
[16] S. Qiao, S. Liu, C. Xiang, G. Fang, and Y. Tan, "Los stabilization model for ship swaying based on subdivision iterative algorithm," *Proc. SPIE*, vol. 10462, pp. 186–192, Mar. 2017.
[17] Y. Wang, "Discussion on coordinates transform of pitch and roll of warship," *Mod. Radar*, vol. 10, no. 4, pp. 27–30, 2001.
[18] J. Zhou, J. Chen, Y. Li, Y. Dong, J. Chen, and Y. Zhao, "Research on target prediction algorithm of ship board photoelectric tracking equipment," *Opt. Precis. Eng.*, vol. 25, no. 2, pp. 519–528, 2017.
[19] D. He, Q. Wang, X. Liu, Z. Song, J. Zhou, Z. Wang, C. Gao, T. Zhang, X. Qi, Y. Tan, G. Ren, and B. Qi, "Shipborne acquisition, tracking, and pointing experimental verifications towards satellite-to-sea laser communication," *Appl. Sci.*, vol. 9, no. 18, p. 3940, Sep. 2019.
[20] C. Peng, D. He, Y. Wang, Y. Huang, X. Liu, L. Yuan, Y. Xu, J. Lei, and H. Ma, "Modeling and correction of pointing errors in gimbals-type optical communication terminals on motion platforms," *IEEE Photon. J.*, vol. 13, no. 3, pp. 1–15, Jun. 2021.

XIN HUANG received the B.E. degree from Southwest Jiaotong University, Chengdu, China, in 2017. He is currently pursuing the Ph.D. degree with the Changchun Institute of Optics, Fine Mechanics and Physics, Chinese Academy of Sciences, China. His main research interests include photoelectric imaging and measurement techniques.

JING WANG is currently a Research Fellow and a Ph.D. Supervisor with the Changchun Institute of Optics, Fine Mechanics and Physics, Chinese Academy of Sciences, China. Her main research interests include optical precision instrument design and photoelectric imaging technology.

DONG WANG received the B.E. degree from Hebei Union University, Tangshan, China, in 2014, and the Ph.D. degree from the Changchun Institute of Optics, Fine Mechanics and Physics, Chinese Academy of Sciences, China. He is currently with the China North Vehicle Research Institute (NCVRI). His main research interest includes the design of compound aircrafts.

JIAHAO PENG received the M.S. degree from Northwestern Polytechnical University, Xi'an, China, in 2014. He is currently pursuing the Ph.D. degree with the Changchun Institute of Optics, Fine Mechanics and Physics, Chinese Academy of Sciences, China. His main research interest includes optimal design of mechanical structure of space camera.

BAO ZHAO received the B.E. degree from the Jilin Institute of Chemical Technology, Changchun, China, in 2018. He is currently pursuing the M.S. degree with the Changchun Institute of Optics, Fine Mechanics and Physics, Chinese Academy of Sciences, China. His main research interests include structural optimization and design of optical measurement equipment.